WATER RESOURCES RESEARCH, VOL. 49, 8357–8369, doi:10.1002/2013WR014259, 2013

Field experiment on alternate bar development in a straight sand-bed stream

J. P. C. Eekhout,[1] A. J. F. Hoitink,[1] and E. Mosselman[2,3]

Received 21 June 2013; revised 12 November 2013; accepted 12 November 2013; published 13 December 2013.

[1] Alternate bars in rivers and streams develop as a result of differences in length scales involved in the adjustment of flow and sediment transport to irregularities of the bed. The amount of field evidence supporting theoretical insights is highly limited. Here, we present results from a large-scale field experiment in a 600 m long straight reach. Over a period of almost 3 years, the channel was allowed to evolve autogenously from initially flat bed conditions, subject to discharge variation. Alternate bars developed within 8 months from the start of the experiment. The initial stages of bar development included bar growth, both in wavelength and amplitude, and bar migration. The latter was too limited to classify the bars as being migrating bars; therefore, we classify the bars as nonmigrating bars. Toward the end of the experiment, the regular alternate bar pattern evolved into an irregular pattern and bar amplitude started to decrease. From the start of the experiment we observed a declining channel slope, from 1.8 m km^{-1} initially to 0.9 m km^{-1} halfway the experiment, after which it stabilized. We applied two bar theories to establish their predictive capacity. Both bar theories predicted the development of alternate bars under the constructed channel conditions. In response to the declining channel slope, both theories predicted a decreasing likelihood for the development of alternate bars. Our study shows that under field conditions, the applied bar theories may predict the initial stages of bed development.

Citation: Eekhout, J. P. C., A. J. F. Hoitink, and E. Mosselman (2013), Field experiment on alternate bar development in a straight sand-bed stream, *Water Resour. Res.*, *49*, 8357–8369, doi:10.1002/2013WR014259.

1. Introduction

[2] Alternate bars in rivers and streams are an instability phenomenon related to differences in the characteristic length scales for the adjustment of flow and sediment transport to irregularities at the channel bed. The vast majority of the experimental support for the existing theory relies on laboratory experiments assuming a constant discharge. Field studies are rare, which causes the practical applicability of existing theory to remain largely unclear. Aiming to verify the predictive capacity of existing bar theory, here, we report on a large-scale field experiment in which alternate bars form under variable discharge conditions.

[3] A key parameter for the development of alternate bars is the width-to-depth ratio of the channel. Alternate bars occur only within a limited range of this ratio. Wider and shallower channels give rise to multiple bars, rather than alternate bars [*Parker*, 1976; *Colombini and Tubino*, 1990]. Narrower and deeper channels do not produce any bars at all [*Struiksma et al*., 1985]. The range for alternate bars can be expected to cover higher width-to-depth ratios in systems of overall erosion and lower ratios in systems of overall sedimentation, because bed degradation reduces the number of bars at a given width-to-depth ratio, whereas bed aggradation increases the number of bars [*Germanoski and Schumm*, 1993]. A linear stability analysis of the mathematical equations provides values of the temporal growth rate, the migration speed, the wavelength, and the spatial damping factor for alternate bars at specific conditions of flow and sediment [*Hansen*, 1967; *Callander*, 1969; *Blondeaux and Seminara*, 1985; *Struiksma et al*., 1985]. Linear stability analysis provides information on how bar amplitudes change in time and space, but not on the values of the amplitudes themselves. The latter can be obtained from weakly nonlinear stability analysis [*Colombini et al*., 1987; *Schielen et al*., 1993]. Theoretically, linear and weakly nonlinear stability analyses apply to infinitesimally small amplitudes only, but experimental findings show they work well for larger amplitudes.

[4] Two special cases arise from two different simplifications of the general linear analysis. *Hansen* [1967], *Callander* [1969], and *Blondeaux and Seminara* [1985] assume that the spatial damping factor is equal to zero, so that all bars have the same height. This implies they assume an infinitely long channel without any influence from

Additional supporting information may be found in the online version of this article.

[1]Hydrology and Quantitative Water Management Group, Wageningen University, Wageningen, Netherlands.
[2]Section of Hydraulic Engineering, Faculty of Civil Engineering and Geosciences, Delft University of Technology, Delft, Netherlands.
[3]Deltares, Delft, Netherlands.

Corresponding author: J. P. C. Eekhout, Hydrology and Quantitative Water Management Group, Wageningen University, Droevendaalsesteeg 3a, NL-6708 PB Wageningen, Netherlands. (joriseekhout@gmail.com)

0043-1397/13/10.1002/2013WR014259

upstream or downstream boundaries. The alternate bars are supposed to start growing spontaneously at the same time everywhere, without any gradients in bar amplitude. The resulting migration speed and wavelength correspond to the bars with the largest temporal growth rate. The alternate bars of this first special case are called migrating bars, migrating free bars or, less precisely but widespread, free bars. *Struiksma et al*. [1985] assumed that the temporal growth rate and the migration rate are equal to zero, which means that the bars neither migrate nor grow or decay in time. This is assumed to correspond to bars that are induced by some local, nonmigrating geometrical forcing, such as a transverse dam in part of the cross-section or an abrupt change in channel curvature. The alternate bars of this second special case are called steady bars, nonmigrating bars, spatial bars or, less precisely but widespread, forced bars. They are significantly longer than the migrating bars [*Olesen*, 1984] and offer an explanation for overdeepening or additional scour along the outer bank of river bends [*Struiksma et al*., 1985; *Parker and Johannesson*, 1989]. Both special cases assume a constant discharge, but *Tubino* [1991] extended the analysis of migrating bars to varying discharges. *Tubino* [1991] showed that bar amplitude varies in response to the rising and falling stages of a flood event. The weakly nonlinear theory predicts the final bar amplitude, after applying the theory to a sequence of typical flood events.

[5] Both migrating bars and nonmigrating bars have been reproduced under laboratory conditions [e.g., *Tubino*, 1991; *Lanzoni*, 2000; *Crosato et al*., 2011; *Venditti et al*., 2012]. Migrating bars occurred in laboratory experiments, even though Blondeaux and Seminara's condition of absent boundaries, or boundaries without any influence, were not met. Nonmigrating bars forced by a local geometrical forcing have also been reproduced in laboratory flumes. These laboratory experiments demonstrate that the equilibrium bed topography that is eventually reached, when the condition of small amplitudes is no longer satisfied, has more or less the same wavelength and spatial damping as the nonmigrating bar pattern formed initially from a flat bed [*Struiksma et al*., 1985]. Long-duration laboratory experiments by *Crosato et al*. [2011] show migrating bars to be transient features that eventually develop into nonmigrating bars if the discharge remains constant. The presence of nonmigrating bars suppresses migrating bars [*Seminara and Tubino*, 1989; *Lisle et al*., 1991], but *Crosato et al*. [2011] argue, nonetheless, that migrating bars could be regenerated episodically if the discharge varies. The slowly evolving nonmigrating bars result most probably from geometrical forcing at the boundaries, because their generation requires a permanent nonmigrating forcing. The convective nature of alternate bars implies that the pattern would disappear from an infinitely long channel after removal of all local geometrical forcing [*Defina*, 2003; *Federici and Seminara*, 2003]. Once a pattern of nonmigrating bars persists, each bar can be seen as a new nonmigrating forcing for the next bar downstream (and upstream in case of a super-resonant width-to-depth ratio). As a result, the bar amplitude eventually becomes uniform along the channel, irrespective of initial spatial variations [*Crosato et al*., 2011].

[6] The vast majority of the experimental support for the existing theory relies on laboratory experiments. Field studies are rare and add complexity to the river system by large discharge variations, bank erosion, heterogeneous sediment, vegetation development and changes in the longitudinal stream profile due to reach-scale erosion and sedimentation. One of the first to report on a field study on alternate-bar behavior was *Lewin* [1976], who investigated the development of alternate bars in a straightened gravel-bed stream (River Ystwyth, Wales) over a period of 1 year. His results are mainly qualitative, however, they give a good overview of the initial stages of bar development in a straight river channel. *Welford* [1994] presented a field experiment on alternate bar behavior in a straightened gravel-bed stream (Embarras River, USA). He tested the alternate bar theory for unsteady flows of *Tubino* [1991] against the results of his field experiment. *Welford* [1994] concluded that the process of bar formation in his field experiment occurred under different flow conditions, and in a different manner than predicted by the *Tubino* [1991] model. *Tubino et al*. [1999] refer to *Welford* [1994] as a properly designed field prototype, concluding that in spite of its approximate character, which mainly resides in the assumption of weak unsteadiness, the model was able to replicate observed trends in bar amplitude and to reproduce the distinct lag between flow variability and bed response exhibited by field observations. Recently, *Rodrigues et al*. [2012] studied two migrating bars in a side channel of the river Loire (France). The side channel was only inundated during flood events. *Rodrigues et al*. [2012] showed the resulting morphodynamics for a single discharge peak, where bar migration was observed during the falling limb of the discharge peak. A field scale experiment was performed by *Venditti et al*. [2012], focusing on alternate bar dynamics under varying sediment supply conditions. They showed that their nonmigrating bars vanished when the sediment supply was terminated. Until now, *Welford* [1994] remains the only field study that actually tested the applicability of existing bar theory.

[7] Here, we present the results from a field experiment, over a period of almost 3 years. The straight channel was allowed to evolve autogenously from initially flat bed conditions, subject to discharge variation, where alternate bars formed over a period of 8 months after the start of the experiment. In our experiment, we observed bar elongation, bar migration, bar amplitude growth, and subsequent bar decay. These processes can be related to both migrating and nonmigrating bars; therefore, we compare our field observations with two lines of research. We evaluate the predictive capacity for the case of migrating bars by the theory of *Tubino* [1991] and for the case of nonmigrating bars with a simple physics-based predictor for the number of river bars [*Crosato and Mosselman*, 2009], which is based on the nonmigrating bar theory by *Struiksma et al*. [1985].

2. Study Area

[8] The stream under study is the Hooge Raam (51°42′56″N, 5°42′7″E), a tributary of the river Meuse (Figure 1a). The catchment (Figure 1b) covers an area of 42.8 km^2. The elevation within the catchment varies between 9 and 22 m above mean sea level. The stream can be characterized as a lowland stream. The average yearly

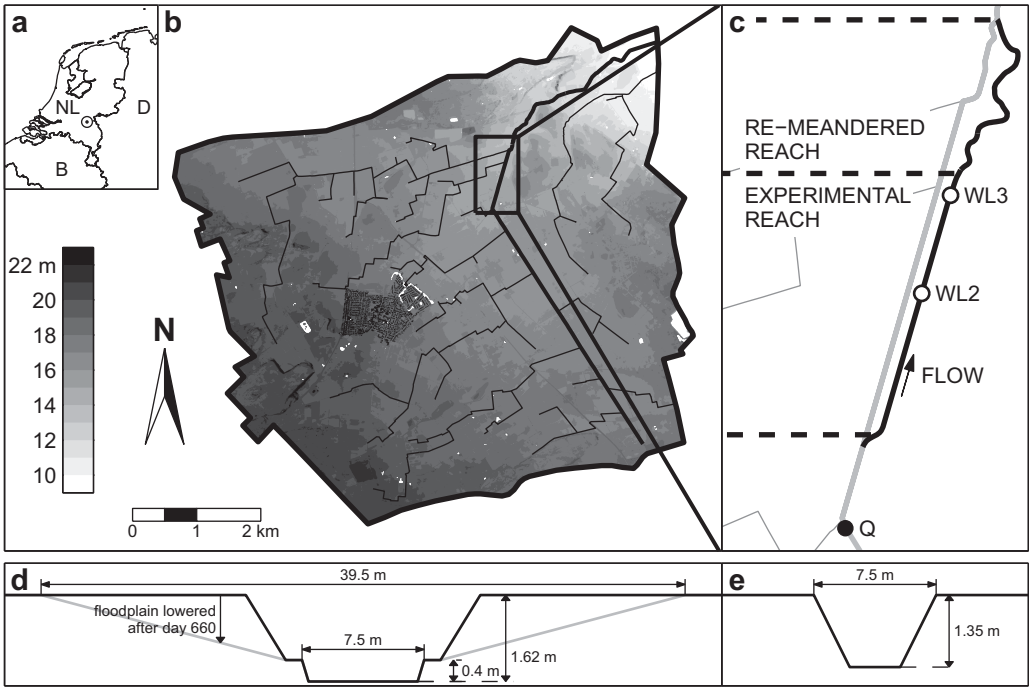

Figure 1. Overview of the study area: (a) geographic location, (b) digital elevation model of the catchment, (c) schematic diagram of the study area, where Q indicates the location of the discharge station and WL2 and WL3 the locations of the water level gauges, (d) design cross-section of the experimental reach, with in gray the floodplain after lowering, and (e) the design cross-section of the re-meandered reach.

precipitation amounts to 777 mm. The subsurface of the catchment mainly consists of drifting-sand deposits. The mean daily discharge is 0.22 $m^3 s^{-1}$ and the peak discharge in the study period was 5.67 $m^3 s^{-1}$ (Figure 2a).

[9] In the summer of 2009, a stream restoration project was completed over a length of about 1 km (Figure 1c). The downstream part of the project was restored by constructing a sinuous channel pattern, based on the historical planform observed on maps dating from the period before straightening. Figure 1e shows the initial channel cross-section of this part of the channel. In the upstream part, a straight channel was created, with the purpose to study autogenous meander initiation. The length of this experimental reach is 600 m, with an initial channel slope of 1.8 m km^{-1}. The channel had a constructed width of 7.5 m and a constructed depth of 0.4 m (Figure 1d). The design was based on general hydraulic geometry relations, established from a comprehensive data set described in *Church and Road* [1983]. The initial channel was constructed 1.2–1.6 m below ground level, due to the upstream and downstream connection with the existing incised channel bed. The initial profile of the cross-section featured a small floodplain

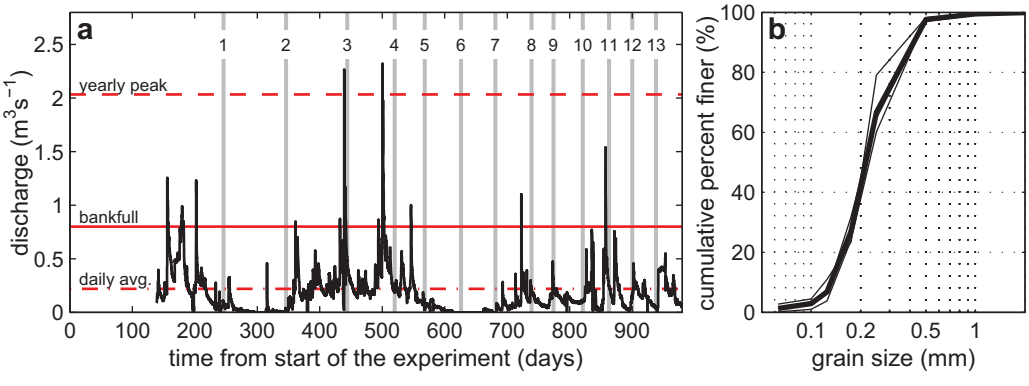

Figure 2. (a) Discharge hydrograph of the channel under study. The red horizontal lines denote the yearly peak discharge (dashed), bankfull discharge under initial constructed channel conditions (solid) and daily average discharge (dash-dotted). The 13 surveys are indicated with the gray vertical lines. (b) Grain size distributions from bed material samples, taken at three locations in the experimental reach. The bold line denotes the average from all three samples.

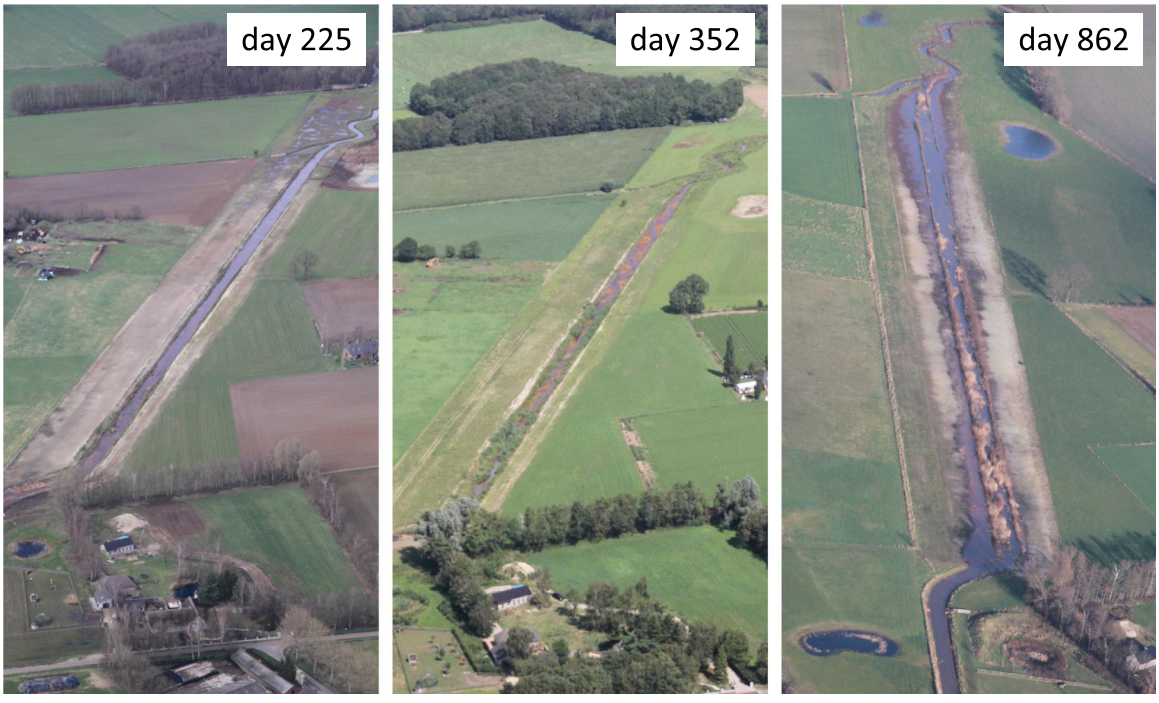

Figure 3. Aerial photos of the experimental reach, taken at 225, 352, and 862 days after the start of the experiment. Water is flowing from the bottom to the top. The middle photo shows a clear difference between the vegetated area (upstream) and the regular pattern of alternate bars (downstream).

section, which was considered too narrow. For this reason, the floodplain was lowered 660 days after the start of the experiment (Figure 1d), creating a better connectivity between the channel bed and the surrounding area, both from a morphological and an ecological perspective. The bed sediment consists of cohesionless fine sands, with a median grain size of 218 μm (Figure 2b).

3. Materials and Methods

[10] The experimental reach has a length of 600 m. Figure 3 shows three aerial photos taken 225, 352, and 862 days after the start of the experiment. Water is flowing from the bottom to the top. The middle photo shows a regular pattern of alternate bars in the downstream part of the experimental reach. In the upstream part, however, dense vegetation growth resulted in an irregular bed morphology, without a clear pattern of alternate bars. The dense vegetation in the upstream part emerged around 320–350 days after the start of the experiment. The break in the development within the two parts of the experimental reach coincides with a border in land ownership. The sudden change in vegetation may relate to differential nutrient supply from the neighboring agricultural lands. In this manuscript, we focus on the morphodynamics of the downstream part, where alternate bars developed, initially unhindered by vegetation growth, over a length of 280 m. The entire 600 m of the experimental reach, including the upstream vegetated part, was surveyed twice, namely just after construction was completed and during the last survey.

[11] Bed elevation data from 13 GPS-surveys were analyzed. Bed elevation data were collected using RTK-GPS equipment (Leica GPS 1200+). The RTK-GPS equipment measures a point in space with an accuracy of 1–2 cm. The number of points collected during each individual survey ranged from 600 to 2250, with an average of 1900 point measurements. Digital Elevation Models (DEMs) of each of the data sets were constructed. To do so, a Triangular Irregular Network (TIN) was made using Delaunay triangulation. Subsequently, the TIN was interpolated on a grid using nearest neighbor interpolation, with a grid spacing of 0.2 m. A grid was used to allow for a quantitative comparison among the serial DEMs. An anisotropy factor of 4 was used within the interpolation routine, to account for the lower density of the collected data in the longitudinal direction. The anisotropy factor was derived by dividing the average distance between the cross-sections (2.8 m) by the average distance between the survey points in cross-sectional direction (0.7 m). The raw morphological data are made available as supporting information.

[12] The temporal evolution of the alternate bars was studied by analysis of three geometrical variables, i.e., the bar wavelength, bar amplitude, and longitudinal bar position. The latter was used to determine the bar migration speed. The bar wavelength and longitudinal bar position were evaluated based on longitudinal bed profiles. From these longitudinal bed profiles local extremes were derived, i.e., bar tops/troughs. This was done by first subtracting the average longitudinal channel slope from the bed topography data. Second, the data were filtered using a LOESS regression algorithm [*Tate et al*., 2005].

[13] The bar wavelength, bar position, bar top, and bar trough are defined in Figure 4. Topographic data from the fifth field survey (day 520) are used in this example. We applied the method to the longitudinal profiles for both sides of the channel. In this example, we show the profile

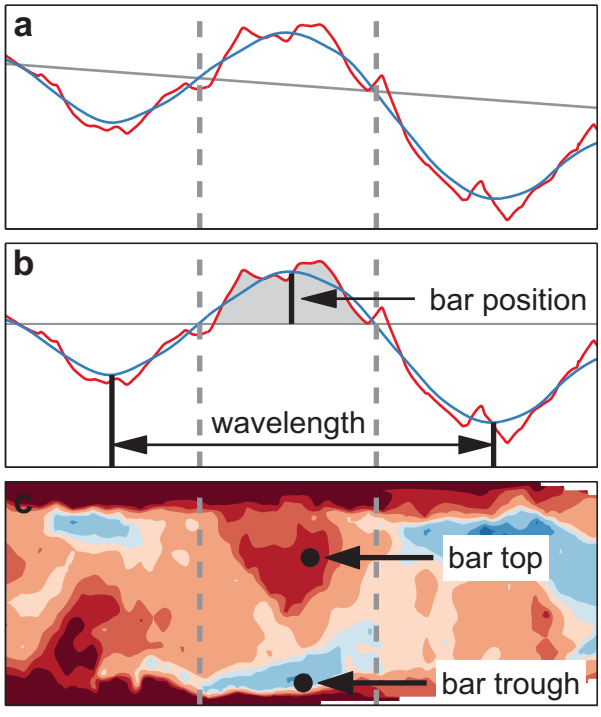

Figure 4. Definition of bar characteristics, with an example of the fifth field survey (day 520): (a) the measured longitudinal bed profile on the left side of the channel (red), the longitudinal bed profile after applying the LOESS regression (blue) and the channel gradient (gray), (b) detrended longitudinal bed profile, and (c) bed topography data. Figure 4b gives definitions for bar wavelength and bar position. Figure 4c gives definitions for the locations of bar top and bar trough, their difference being the bar amplitude.

on the left side. Figure 4a includes the measured longitudinal bed profile, the LOESS filtered longitudinal bed profile, and the channel gradient. Figure 4b shows the longitudinal bed profile after detrending the bed topography by removing the channel slope, in which zero-crossings can easily be detected. Figure 4b illustrates the adopted definitions of bar wavelength and longitudinal bar position. The bar wavelength is defined as the length between two successive bar troughs. The longitudinal bar position is defined by the center of gravity above the average channel slope, defined as:

$$\mathrm{pos}_j = \frac{\sum_{Z_{2,j}}^{Z_{1,j}} (s_{i,j} - Z_{1,j}) \eta_{i,j} \Delta s}{\sum_{Z_{2,j}}^{Z_{1,j}} \eta_{i,j} \Delta s} + Z_{1,j} \qquad (1)$$

where pos_j is the location of bar j, $Z_{1,j}$ and $Z_{2,j}$ are zero-crossings and $s_{i,j}$ is the location of a certain cell i with elevation $\eta_{i,j}$ and width Δs. The width Δs is equal to the grid spacing of 0.2 m.

[14] The longitudinal bar position is used to determine the bar migration speed. The bar migration speed is determined by the bar migration distance divided by the time between two successive surveys ($\Delta \mathrm{pos}/\Delta t$). Bar elongation was observed during the experiment. Therefore, we also determined the resulting longitudinal bar growth, which is defined as the difference in bar wavelength between two successive surveys divided by the time between the two surveys ($\Delta \lambda/\Delta t$).

[15] Figure 4c shows the bed topography from the fifth field survey. The bar amplitude is determined by the difference between the local maximum and local minimum, within the area between two zero-crossings and the channel banks. The local maximum and local minimum represent the bar crest and bar trough of a particular bar, respectively.

[16] Discharge data were collected upstream of the experimental reach at a discharge measurement weir, marked by Q in Figure 1c. The discharge measurement weir was operational from day 140 until the end of the experiment. Discharge data were collected with a one hour frequency. Water level data were measured at two locations along the experimental channel, marked as WL2 and WL3 in Figure 1c, located at 325 and 547 m from the upstream end of the experimental reach, respectively. The water level gauges were operational from day 660 until the end of the experiment. Water level data were collected with a one hour frequency. Longitudinal water level profiles were measured during 6 of the 13 surveys. During the 11th field survey (day 863), we observed a clear mark indicating the highest water level in the preceding period. The date and time of this high-water event could be traced back from the measured water level time-series at the two water level gauges. The raw

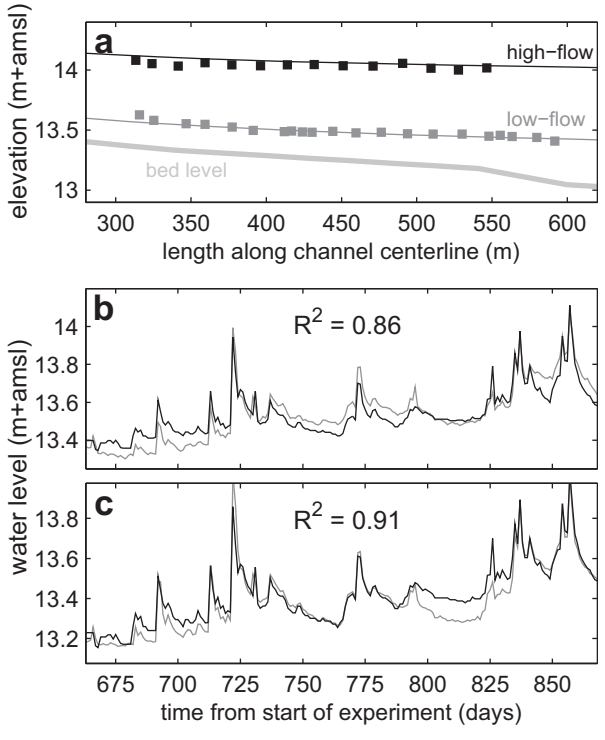

Figure 5. Results from (a) model calibration and (b and c) model validation. The squares in Figure 5a denote the measured water levels during the survey and the lines the modeled water levels. The thick light gray line denotes the bed level. Figures 5b and 5c show the validation results for the water level gauges WL2 and WL3, located at $x = 325$ m and $x = 547$ m, respectively. The gray lines represent the measured water levels and the black lines represent the modeled water levels.

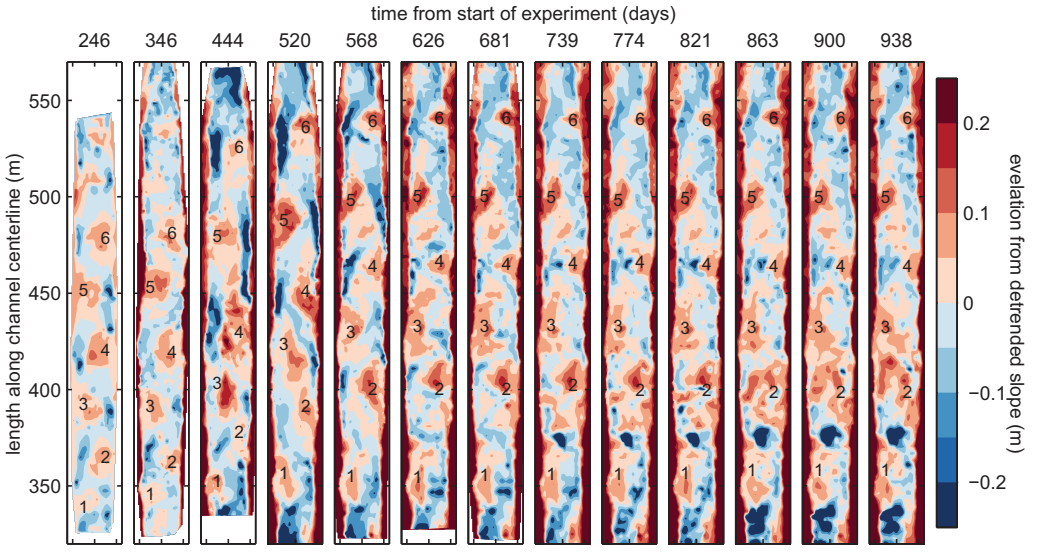

Figure 6. Detrended bed topography data from the 13 GPS-surveys. The numbers indicate the location of the six individual bars. Water is flowing from bottom to top.

hydrological data are made available as supporting information.

[17] The cross-section averaged flow velocity in the experimental reach was obtained from discharge and an estimation of hydraulic roughness, using a model implementation of the Saint Venant equations [SOBEK Channel flow, *Deltares*, 2011]. Longitudinal water level measurements revealed an M1-backwater curve (see Figure 5a), caused by the narrower cross-sectional shape near the downstream end of the study reach (compare Figures 1d and 1e). The backwater curve causes the flow velocities to slightly decrease in the downstream direction.

[18] In the hydrodynamic modeling exercise, we took into account the temporal changes of the channel dimensions, i.e., variation of the channel slope and the floodplain lowering after day 660. Discharge was imposed at the upstream boundary and water level at the downstream boundary. The hydrodynamic model was calibrated using measured longitudinal water level profiles. A low-flow case (day 774, $Q = 0.22$ m^3 s^{-1}) and a high-flow case (high-water mark at day 857, $Q = 1.73$ m^3 s^{-1}) were selected from the available observed longitudinal water level profiles. The calibration was performed by adjusting the bed and floodplain roughness values, which yielded optimal Chézy values of 13 and 10 m$^{1/2}$ s^{-1}, respectively. The Chézy value in the floodplain was attributed a lower value to represent the presence of vegetation. Figure 5a shows the results of the calibration procedure. The hydrodynamic model was validated using the measured water level time-series (Figures 5b and 5c). The modeled water level time-series at both locations compare well with the measurements ($R^2 = 0.86$ for the upstream and $R^2 = 0.91$ for the downstream location). Both panels show the highest degree of agreement during periods of high flow. Low flows are either under or overpredicted.

4. Experimental Results

[19] First, we present the results from the 13 morphological surveys. The first survey was performed 246 days after the start of the experiment. Figure 6 shows the bed topography data of the morphological surveys. For the first five surveys, the individual bars can be distinguished relatively easily. At the fifth survey, a more or less sinuous thalweg appears in the channel. The alternate bars grow both in length and in amplitude in the first five surveys. As time evolves, the morphology of the channel increases in complexity. The alternate bars become repeatedly connected and disconnected from each other, and from day 739 onward several scour holes appear in the channel in the upstream part of the experimental reach, around 325 and 380 m from the upstream end of the study reach.

[20] In total, six bars were identified that appear in the data from the 13 surveys, i.e., three on the left side and three on the right side of the channel. The most downstream bar was excluded from the analysis, because it was possibly affected by the downstream boundary. Figure 7 shows the temporal evolution of the bar wavelength and the bar amplitude of the five bars. The bar wavelength initially

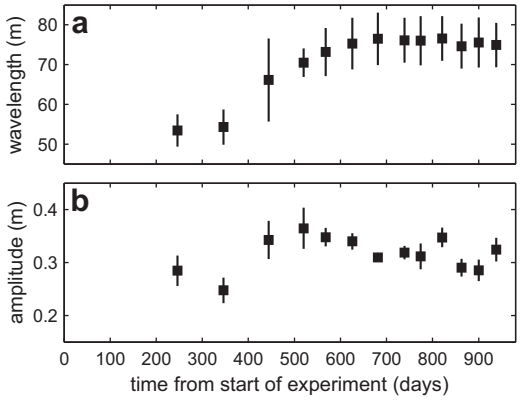

Figure 7. Evolution of (a) the average bar wavelength and (b) the average bar amplitude from the five bars. The length of the error bars is defined as the standard deviation divided by the square root of the number of bars ($\sigma/\sqrt{n}$).

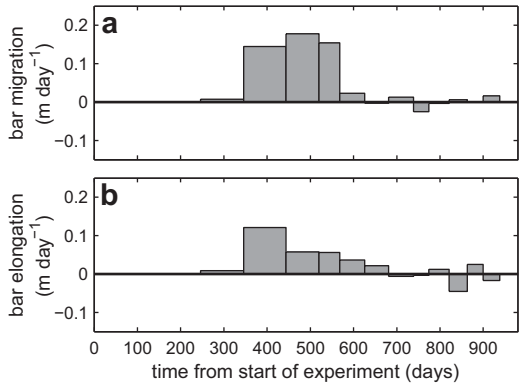

Figure 8. Evolution of the (a) bar migration and (b) bar elongation.

increases in time up until the fifth survey, after which an equilibrium wavelength is reached, averaging 75.7 m. The evolution of the bar amplitude is more irregular. The bar amplitude decreases from the first to the second survey and increases from the second to the fourth survey. At the fourth survey, the maximum average bar amplitude is reached, amounting to 38.3 cm. After the fourth survey, a downward sloping trend is visible, with slight increases of bar amplitude only around the 10th and 13th surveys. The latter is mainly caused by the irregular topography at the end of the experiment (Figure 6), which complicated the identification of local extremes, needed to describe the bar tops and bar troughs.

[21] Figure 8 shows the bar migration and bar elongation for the 12 survey intervals. Figure 8a shows bar migration occurred especially between day 346 and day 568, with an average bar migration speed of 0.17 m day^{-1} in this period. Bar elongation was restricted to the period between day 346 and day 681. This period of bar elongation largely overlaps the period of bar migration. In addition, bar migration rates are of the same order of magnitude as the bar elongation rates. We arguably interpret the observed bar migration as a side effect of bar elongation, rather than actual bar migration.

[22] Figure 9a shows the average cross-sectional bed level for the experimental reach, just after construction was realized (day 0) and at the end of the experiment (day 938). The figure shows an overall decline of the bed slope. Where the longitudinal profile initially had an average slope of 1.8 m km^{-1}, it decreased to 0.9 m km^{-1} after 938 days. Figure 9b shows the development of the channel slope in the downstream part of the experimental reach. The channel slope decline occurred gradually from the start of the experiment until day 520, after which it stabilized. The channel slope decline is most probably caused by a backwater effect, which we observed during several morphological surveys. The right-most aerial photo of Figure 3 shows that at the downstream end of the experimental reach (upper part of the photo) water inundates the floodplain, a result of the backwater effect.

[23] Figure 10 shows cross-sections at successive bar tops, for surveys carried out immediately after construction of the stream, at day 520 and at day 938. All panels show both aggradation of the channel bed and erosion of the channel banks from the start of the experiment until day 520. Aggradation of the bed is most apparent for the bars located in the downstream section of the experimental reach, summing up to 0.30 m for both bars 2 and 3. Erosion of the channel banks is apparent at all individual bar locations. Channel bank erosion shows the highest rates for bar 3, which amounts to more than 1 m over 520 days. Morphological changes between days 520 and 938 are mainly restricted to sedimentation of the bar troughs, up to 0.10 m for bar 3. This holds for all bars except for bar 5, which hardly shows any morphological change between days 520 and 938. Sedimentation of the bar troughs explains the decrease of bar amplitude, as shown in Figure 7b.

[24] Table 1 summarizes some of the results obtained from the field experiment. Both the average discharge and the average water depth reflect the seasonal variation, as shown in Figure 2a. The response of the flow to the declining channel slope is mainly reflected in the average flow velocity, average Shields parameter and average Froude number. Each of these three flow characteristics show decreasing values in response to the declining channel slope.

5. Predictive Capacity of Existing Bar Theory

[25] Theoretical models by *Tubino* [1991] and *Struiksma et al*. [1985] have the potential to predict the occurrence of migrating bars and nonmigrating bars, respectively. The input for both models is basically restricted to flow velocity, grain size, channel width, channel depth, and channel slope. We applied the bar models by adopting the reach average flow velocities obtained from the 1-D-flow model. Since both theoretical models assume uniform flow conditions, the application to the gradually varied flow of this case may seem inconsistent, but the observed rhythmic pattern of the five

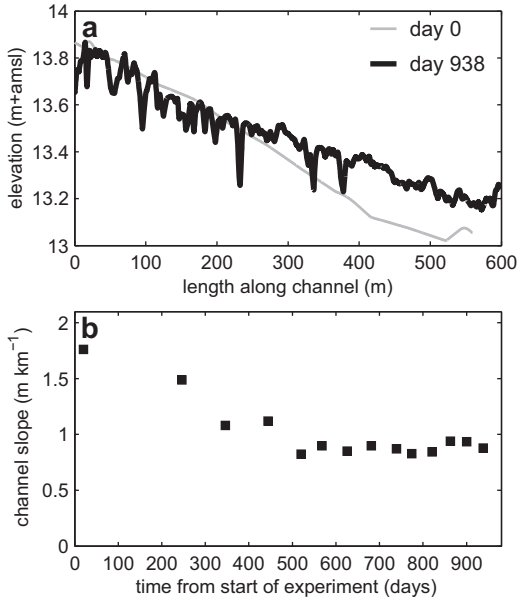

Figure 9. (a) The longitudinal bed profile just after construction (gray) and after 938 days from the start of the experiment (black). The black line shows increased bed levels in the downstream part of the channel, causing a reduction of the longitudinal bed slope. (b) The temporal evolution of the channel slope in the downstream part of the experimental reach.

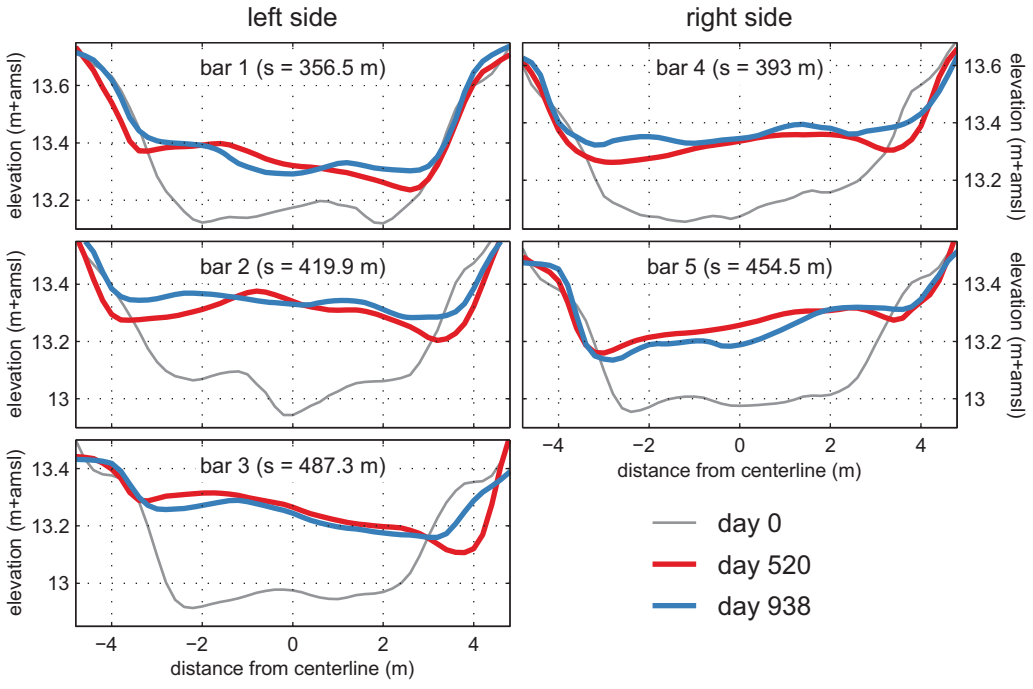

Figure 10. Channel cross-sections at each of the five bars from three surveys: just after construction (gray), at day 520 (red) and at day 938 (blue). The figure shows sedimentation over the full width of the channel from the start of the experiment. Additionally, sediment is deposited in the bar troughs in the period between day 520 and day 938.

retained alternate bars does not show any systematic trends that can be interpreted as signs of a backwater effect.

5.1. Theory by *Tubino* [1991]

[26] The model of *Tubino* [1991] simulates migrating bar development in response to a varying discharge. The model predicts bar dynamics under unsteady flow conditions. Here, we limit our analysis to the temporal dynamics of the unsteadiness parameter, which is directly linked to the occurrence of migrating bars. This results in a quasi-steady analysis, in which we define a reference state for each of the 13 surveys separately. The reference state is defined by three dimensionless parameters, i.e., the mean width-to-depth ratio $\tilde{\beta}$, the mean roughness parameter $\tilde{d}_{50}$, and the mean Shields parameter $\tilde{\theta}$ (dimensionless variables are denoted with a tilde):

$$\tilde{\beta}=\frac{0.5B}{\overline{h}_0} \tag{2}$$

$$\tilde{d}_{50}=\frac{d_{50}}{\overline{h}_0} \tag{3}$$

$$\tilde{\theta}=\frac{S}{\Delta\tilde{d}_{50}} \tag{4}$$

where B is the width of the channel, $\overline{h}_0$ is the reach-averaged flow depth (in the reference state), d_{50} is the median grain size, S is the bed slope, and $\Delta=(\rho_s-\rho)/\rho$ is the relative submerged specific gravity of the sediment. For the case study presented here, we attribute $B=7.5$ m and $d_{50}=218$ μm.

[27] The reference state is selected by choosing a set of parameters satisfying the following two conditions:

$$\tilde{\varepsilon}(\tilde{\theta},\tilde{d}_{50})=\frac{\tilde{\beta}-\tilde{\beta}_c(\tilde{\theta},\tilde{d}_{50})}{\tilde{\beta}_c(\tilde{\theta},\tilde{d}_{50})}=\tilde{\delta} \tag{5}$$

$$\tilde{q}_{th}(\tilde{\theta},\tilde{d}_{50})=\frac{q_{th}}{\overline{q}_0}(\tilde{\theta},\tilde{d}_{50})=1-\tilde{\delta} \tag{6}$$

where $\tilde{\varepsilon}$ and $\tilde{\delta}$ are perturbation parameters, $\tilde{\beta}_c(\tilde{\theta},\tilde{d}_{50})$ is the critical value of the width-to-depth ratio for the formation of migrating alternate bars, $\overline{q}_0(\tilde{\theta},\tilde{d}_{50})$ is the average flow discharge per unit width, q_{th} is the minimum value of $\overline{q}_0(\tilde{\theta},\tilde{d}_{50})$, and $\tilde{q}_{th}(\tilde{\theta},\tilde{d}_{50})$ is the dimensionless value of q_{th}.

[28] Values of $\tilde{\beta}_c$ are obtained from Figure 11a, which shows $\tilde{\beta}_c$ as a function of $\tilde{\theta}$ and $\tilde{d}_{50}$ based on the idealized model. We used the minimum value of the discharge, because the flow conditions nearly permanently exceed the threshold for sediment motion. From the discharge time series, 13 flood waves were identified, with peak values exceeding 0.8 $m^3\ s^{-1}$, i.e., the bankfull discharge under constructed channel conditions (at day 0). Accordingly, q_{th} was set to the minimum discharge recorded during these flood waves, which amounted to $Q_{\text{min}}=0.064 m^3 s^{-1}$, and hence, $q_{\text{th}}=Q_{\text{min}}/0.5B=0.017 m^2 s^{-1}$.

[29] The unsteadiness of the flow and morphology can be quantified based on the unsteadiness parameter $\tilde{U}$, which is defined as:

$$\tilde{U}=\frac{\tilde{\sigma}}{\tilde{\varepsilon}\tilde{\alpha}_{1R}} \tag{7}$$

where $\tilde{\sigma}$ is the dimensionless angular frequency of the flood wave and $\tilde{\alpha}_{1R}$ the linear growth rate of bar amplitude on the slow time scale associated with bar development. The dimensionless angular frequency of the flood wave $\tilde{\sigma}$ is

Table 1. Characteristics From the Periods Between the 13 Successive Surveys

From (day)	To (day)	Average Discharge ($m^3\ s^{-1}$)	Average Water Depth (m)	Average Flow Velocity[a] ($m\ s^{-1}$)	Channel Slope ($m\ km^{-1}$)	Average Shields Parameter[b] (–)	Average Froude Number[c] (–)	Width-to-Depth Ratio[d] (–)
0	246	0.29	0.27	0.17	1.80	1.36	0.11	18.6
246	346	0.02	0.04	0.14	1.49	0.17	0.12	19.7
346	444	0.26	0.26	0.14	1.08	0.78	0.09	16.8
444	520	0.34	0.31	0.15	1.12	0.97	0.09	17.0
520	568	0.23	0.28	0.11	0.82	0.64	0.07	14.8
568	626	0.04	0.07	0.09	0.90	0.18	0.08	15.1
626	681	0.00	0.01	0.02	0.85	0.03	0.02	15.5
681	739	0.11	0.16	0.10	0.90	0.39	0.08	15.6
739	774	0.11	0.17	0.11	0.87	0.41	0.08	15.8
774	821	0.13	0.23	0.12	0.83	0.52	0.08	15.5
821	863	0.21	0.36	0.13	0.84	0.85	0.07	15.6
863	900	0.16	0.21	0.11	0.94	0.54	0.08	15.2
900	938	0.16	0.21	0.12	0.94	0.56	0.08	15.5

[a]From 1-D-flow model.
[b]$\theta=\tau/C^2 d_{50}\Delta$, with $\tau=u^2\rho g/C^2$, $C=13\ m^{1/2}\ s^{-1}$, $d_{50}=218\ \mu m$ and $\Delta=1.65$.
[c]$Fr=u/\sqrt{gh}$.
[d]Determined at bankfull discharge (constructed channel), $Q=0.8\ m^3\ s^{-1}$.

expressed as a ratio between the average travel time along the channel reach and the characteristic period of the flood, defined as:

$$\tilde{\sigma}=\frac{\sigma 0.5B}{\overline{u}_0} \tag{8}$$

where $\sigma=2\pi/\tau$ is the angular frequency of the flood wave, with τ the characteristic rise time of the flood wave. We derived the characteristic rise time of the flood wave from the discharge time series. From the 13 selected flood waves, the average rise time amounted to 22 h. The linear growth rate of the bar amplitude $\tilde{\alpha}_{1R}$ is obtained from Figure 11b, which shows $\tilde{\alpha}_{1R}$ for different values of both $\tilde{\theta}$ and $\tilde{d}_{50}$.

[30] Figure 12 shows the unsteadiness parameter $\tilde{U}$ for all surveys. For each survey we obtained the bed slope S and we used the 1-D-flow model results and reference conditions defined by equations (5) and (6) to obtain $\overline{u}_0$ and $\overline{h}_0$. Positive/negative values of $\tilde{U}$ are controlled by the perturbation parameter $\tilde{\varepsilon}$, since $\tilde{\sigma}$ and $\tilde{\alpha}_{1R}$ are always positive. The perturbation parameter $\tilde{\varepsilon}$ becomes positive/negative when $\tilde{\beta}$ is larger/smaller than $\tilde{\beta}_c(\tilde{\theta},\tilde{d}_{50})$, which corresponds to the unstable/stable regime, respectively. The unstable regime corresponds to conditions where migrating bars develop. The stable regime corresponds to conditions where migrating bars do not develop or vanish. In the unstable regime, three subregimes can be identified based on $\tilde{U}$, controlled by the dimensionless angular frequency of the flood wave $\tilde{\sigma}$: (1) $\tilde{U}\sim\mathcal{O}(1)$, bar development is affected by flow unsteadiness; (2) $\tilde{U}\gg 1$, bars develop on a much longer time scale than that associated with the flow unsteadiness; (3) $\tilde{U}\ll 1$, bars develop on a much shorter time scale than that associated with the flow unsteadiness.

[31] Figure 12 shows that the unsteadiness parameter was positive during all surveys, corresponding to the migrating bar regime. Immediately after construction of the channel, conditions corresponded to the first subregime, i.e., $\tilde{U}\sim\mathcal{O}(1)$. This implies that at the start of the experiment, the time scale of migrating bar development was expected to be similar to the time scale of flow variation. Soon after construction, conditions gradually developed toward the second regime, i.e., $\tilde{U}\gg 1$, in which the time scale of migrating bar development is larger than the characteristic time scale of flow variation.

[32] Here, we restricted our analysis to the unsteadiness parameter, whereas the theory by Tubino also presents expressions for bar amplitude and bar wavelength. Efforts to quantify bar amplitude and bar wavelength were hampered by: (1) the apparent focus on gravel-bed rivers,

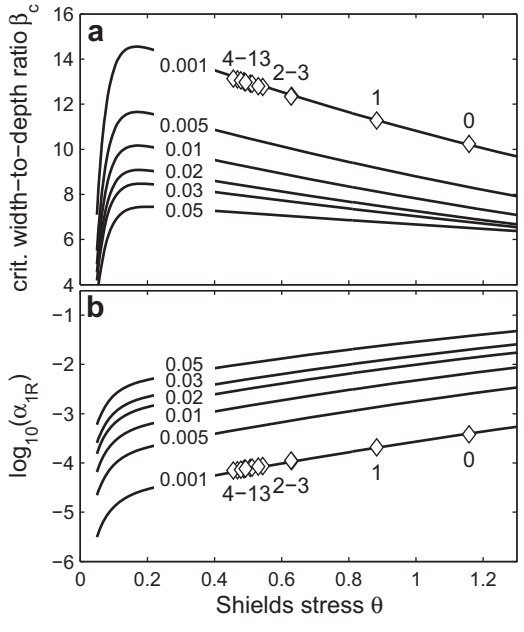

Figure 11. (a) The critical value of the width-to-depth ratio $\tilde{\beta}_c$ above which migrating bars can develop. (b) The linear growth rate of bar amplitude on the slow time scale associated with bar development $\tilde{\alpha}_{1R}$. Both $\tilde{\beta}_c$ and $\tilde{\alpha}_{1R}$ are plotted against the Shields stress θ for six values of the roughness parameter $\tilde{d}_{50}$. The markers $\diamond$ show the values for $\tilde{\beta}_c$ and $\tilde{\alpha}_{1R}$ we obtained for the constructed conditions (0) and conditions for each survey (1–13). Solid lines are adopted from *Tubino* [1991]; $\tilde{\beta}_c$ and $\tilde{\alpha}_{1R}$ are extrapolated for the Shields stress $\tilde{\theta}>0.5$.

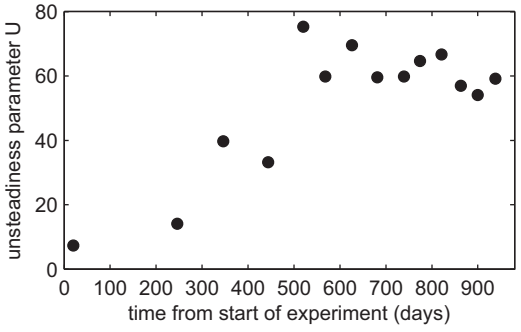

Figure 12. Temporal evolution of the unsteadiness parameter $\tilde{U}$, which is used to determine the different regimes of migrating bar development.

which explains the limited Shields domain for which results are presented ($\tilde{\theta} < 0.5$), and (2) the lack of information on the imaginary parts of the model parameters.

5.2. Theory by *Struiksma et al.* [1985] and *Crosato and Mosselman* [2009]

[33] The physics-based second-order linear model by *Struiksma et al*. [1985] predicts wavelength and spatial damping of bar formation. *Struiksma et al*. [1985] assumed that the temporal growth rate and the migration rate are equal to zero. We applied the theory using the same parameter values as in the Tubino model, except for the discharge, by adopting bankfull discharge conditions, following *Crosato and Mosselman* [2009], and except for the bed slope effect on sediment transport direction, by employing formulations by *Talmon et al*. [1995].

[34] The bar regime can be computed adopting the longitudinal damping coefficient of nonmigrating bars L_D. The system complies with Blondeaux and Seminara's resonant conditions when this coefficient equals zero. When the coefficient is positive/negative, the system is subresonant/super-resonant, respectively. The longitudinal damping coefficient reads:

$$\frac{\lambda_w}{L_D} = \frac{1}{2}\left(\frac{\lambda_w}{\lambda_s} - \frac{b-3}{2}\right) \tag{9}$$

where λ_w is the adaptation length of the flow, λ_s is the adaptation length of a bed disturbance, and b is the degree of nonlinearity in the relation between sediment transport and depth-averaged flow velocity, which is equal to the exponent in case of a power law dependence $q_s \propto u^b$. We attribute $b = 4$, corresponding to a value used for sand-bed rivers, following *Crosato and Mosselman* [2009] and *Kleinhans and van den Berg* [2011].

[35] The adaptation length of the flow λ_w characterizes the longitudinal distance needed for the decay of perturbations in the transverse distribution of flow velocity, generated by an upstream disturbance. The adaptation length for the flow is formulated as:

$$\lambda_w = \frac{\overline{h}_0}{2C_f} \tag{10}$$

where $\overline{h}_0$ is the reach-averaged water depth, derived from the 1-D-flow model results, C_f is the friction factor defined by $C_f = g/C^2$, in which $g = 9.81\,\mathrm{m\,s^{-2}}$ is the gravitational acceleration in the Netherlands, and C the Chézy coefficient set to 13 $\mathrm{m^{1/2}\ s^{-1}}$, which is adopted from the 1-D-flow model.

[36] The adaptation length of a bed perturbation λ_s characterizes the longitudinal distance needed for the decay of perturbations in the lateral water depth profile created by an upstream disturbance, which is defined as:

$$\lambda_s = \frac{1}{\pi^2} h_0 \left(\frac{B}{\overline{h}_0}\right)^2 f(\theta_0) \tag{11}$$

where B is the channel width and $f(\theta_0)$ accounts for the effect of gravity on the direction of sediment transport over transverse bed slopes, which is formulated as [*Talmon et al*., 1995]:

$$f(\theta_0) = 9\left(\frac{D_{50}}{\overline{h}_0}\right)^{0.3} \sqrt{\theta_0} \tag{12}$$

where θ_0 is the reach-averaged value of the Shields parameter, defined by:

$$\theta_0 = \frac{\overline{u}^2}{C^2 \Delta D_{50}} \tag{13}$$

and $\overline{u}$ is the reach-averaged flow velocity, derived from the 1-D-flow model results.

[37] The wavelength (L_P) of nonmigrating bars is formulated as follows:

$$\frac{2\pi}{L_P} = \frac{1}{\lambda_w}\left(\frac{\lambda_w}{\lambda_s} - \left(\frac{\lambda_w}{L_D}\right)^2\right)^{1/2} \tag{14}$$

[38] *Crosato and Mosselman* [2009] derived a predictor for the number of bars per cross-section from the theory by *Struiksma et al*. [1985]. For a river with a width-to-depth ratio β, the bar mode m of the incipient bars can be determined by:

$$m = \frac{\beta}{\pi}\sqrt{(b-3) f(\theta_0) C_f} \tag{15}$$

where the nearest integer of bar mode m relates to the most probable number of bars per cross-section. A bar mode $0.5 < m \leq 1.5$ suggests a series of alternate bars.

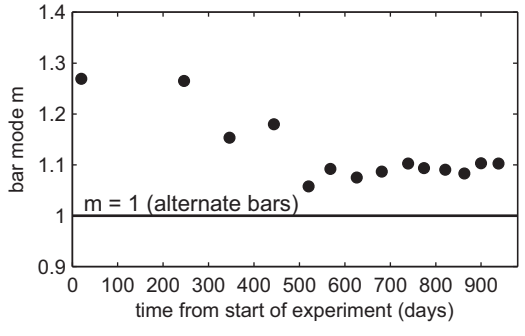

Figure 13. Temporal evolution of the bar mode m.

[39] Figure 13 shows the results for the bar mode m, which describes the bar regime. Equation (15) predicts values around 1, which corresponds to a bar mode with alternate bars. The temporal evolution of m shows a decreasing likelihood of the development of nonmigrating bars, which is shown in Figure 13 by a decrease of m. Similar to the results from the Tubino model, this is mainly caused by the decreasing channel slope.

6. Discussion

[40] The first stages of bar development in the experiment show strong similarities with the field description by *Lewin* [1976] and the numerical model results of *Defina* [2003]. *Lewin* [1976] offers a clear view on the first stages of bar growth in a coarse grained channel bed. He showed that initially, alternate bars developed with bar wavelengths corresponding to three times the channel width. In a subsequent stage, these bars developed into alternate bars with a wavelength of 7.5 times the channel width. The alternate bars migrated in downstream direction during exceptionally high flows. The evolution of the bar amplitude was not reported. *Defina* [2003] developed a numerical model to study alternate bar dynamics and applied the model to the steady flow experiments described by *Lanzoni* [2000], showing initial bar elongation and an increase of bar amplitude. The results show that especially bar amplitude developed toward an equilibrium value. Figure 14 presents a cartoon summarizing the wavelength, amplitude, and migration development of the bars in the present experiment. Combining results from *Lewin* [1976], *Defina* [2003] and our study, which feature contrasting conditions of bar material, elongation of alternate bars may be a general feature occurring in the initial stages of bar development.

[41] The bar development summarized in Figure 14 is markedly different from the results presented by *Welford* [1994]. *Welford* [1994] showed migrating bars formed during the falling limb of a single discharge peak, which vanished during the subsequent periods of low flow. Alternate bars developed sequentially, rather than uniformly, as in our experiment. *Welford* [1994] classified the discharge regime in the straightened section of the Emberras River based on an annual coefficient of flow variation [*Poff and Ward*, 1989]. The latter coefficient amounted to 52.6, which classified the discharge regime in the transition between intermittent runoff and perennial runoff. In the case of the Hooge Raam, the annual coefficient of flow variation amounts to 119.5, corresponding to an intermittent flashy to harsh intermittent discharge regime. While *Welford* [1994] classified the flow variability in the system as fairly high, in our case the flow variability was even higher. In the Tubino model, this flow variability is captured in the characteristic rise time of the flood wave. A flashy discharge regime with high flow variability results in short rise times. This causes an increase of the unsteadiness parameter $\tilde{U}$, which reduces the likelihood of the occurrence of migrating bars. In our field case, this corollary may explain the absence of migrating bars. Flashy discharge hydrographs are typical for highly modified lowland catchments, like in The Netherlands. Migrating bars are not likely to appear under these conditions.

[42] Despite several differences in the underlying assumptions, the theoretical models by *Tubino* [1991] and *Struiksma et al*. [1985] both contain a capacity to predict the main bar developments as observed. Both models predict the occurrence of alternate bars immediately after construction of the channel, and both models predict that the conditions for the bars to prevail become increasingly unfavorable in time. Migrating bars are characterized by a smaller wavelength compared to nonmigrating bars and are typically migrating in the downstream direction. The laboratory experiments described in *Tubino* [1991], used to validate the model, show migration speeds of about 10 bar wavelengths per day. We observed migration speeds of 0.17 m per day, which is equal to 3×10^{-3} bar wavelengths per day. These small migration rates and the coincidence between bar migration and bar elongation suggest that the alternate bars can be classified as nonmigrating. It is plausible that migrating bars have triggered the start of bar development in the initial stage of the experiment. From the second survey onward, the Tubino model predicts the time scale of migrating bar development to become much larger than the time scale of the flow variation ($\tilde{U} \gg 1$). The model may be correct in reproducing the observation, but the information available is insufficient to establish the model performance rigorously.

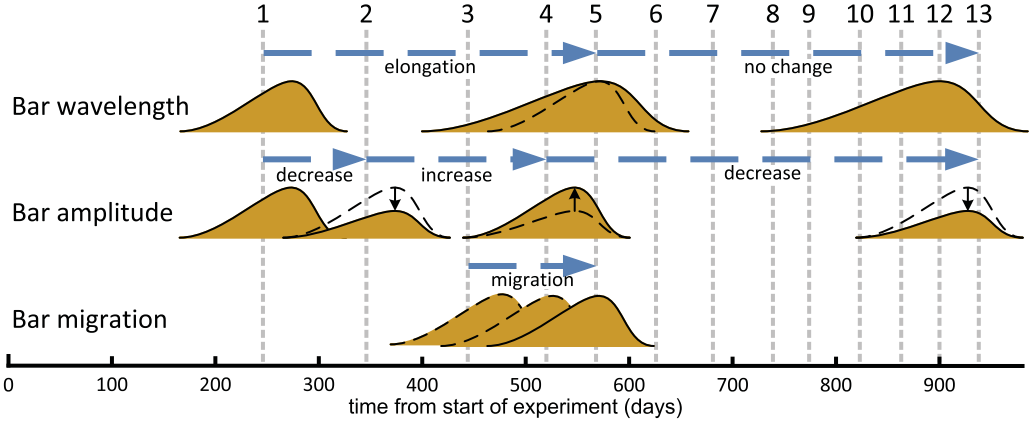

Figure 14. Schematic diagram of the temporal evolution of bar wavelength, bar amplitude and bar migration.

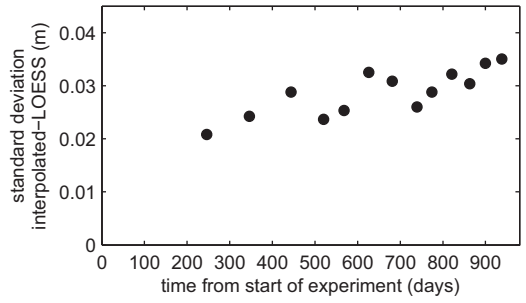

Figure 15. Standard deviation of the difference between the raw bed elevation data and corresponding LOESS filtered data.

[43] The results from our field experiment show an initially regular alternate bar pattern until halfway the experiment. In the second half of the experiment, the regular bar pattern evolved to become irregular. To quantify the increased irregularity of the bed topography, we subtracted the raw bed elevation data from the filtered elevation data. Figure 15 shows an increase of the standard deviation of these residuals from around 0.020 to 0.035 m. We argue that the bed forms in the final stages of the experiment are merely relics from initially regular bar pattern. Figure 16 shows how vegetation cover increases toward the end of the experiment. The vegetation cover on the bars may be responsible for stabilizing the initial bar pattern.

[44] The Crosato and Mosselman model predicts the development of nonmigrating alternate bars throughout the experiment, with values for bar mode m around 1, suggesting bars to prevail during the entire experiment. The bar mode m shows a tendency to decrease toward $m = 1$, caused by the declining channel slope. This could be interpreted as a decreasing likelihood of alternate bar development. In a recent study, *Venditti et al*. [2012] showed that termination of upstream sediment supply caused alternate bars to disappear, both under laboratory and field conditions. In their field experiment, the channel slope reduced to half the initial value, with the main longitudinal adjustment being upstream erosion. In our experiment, channel slope decline was mainly caused by downstream deposition of sediment. The end result is similar for both cases: a decreased regularity of the initial alternate bar pattern.

[45] The theoretical bar models we applied in this case study assume uniform flow and channel bed conditions. The field results show that these conditions were not met during the entire study period. A backwater effect is held responsible for the declining bed slope, hence, flow was not uniform over the whole length of the experimental reach. Besides, the experimental reach was subject to a flashy discharge hydrograph. Most of the time, the flow conditions did not correspond to the average flow conditions, as used in the two bar theories. Furthermore, the vegetated upstream part of the experimental reach may have had an influence on the sediment supply to the downstream part. These constraints may have influenced bar dynamics and may also explain the deviation between field observations and model results, near the end of the experiment. A logical next step would be to apply a numerical model to this case study, to study these constraints in more detail.

7. Conclusions

[46] We presented the results from a field experiment where alternate bars developed within 8 months after the start of the experiment. From the obtained field data a sharp view on the initial increase of bar wavelength and bar amplitude was obtained. These findings are consistent with existing field studies on alternate bars, suggesting that the growth and elongation of alternate bars may be a general feature occurring in the initial stages of bar development. A period of bar migration was recorded, which coincided with the period of bar elongation. The migration rates were several orders of magnitude smaller than those presented previously in laboratory experiments. This suggests the observed alternate bars can be classified as nonmigrating bars, rather than migrating bars.

[47] Using the obtained data set, the predictive capacity of two bar theories was established: (1) the theory by *Tubino* [1991] for migrating bars and (2) the theory by *Struiksma et al*. [1985] and *Crosato and Mosselman* [2009] for nonmigrating bars. Both theories predicted the occurrence of alternate bars under the constructed channel conditions. Halfway the experiment, the regular pattern of alternate bars evolved into an irregular bed topography, and bar amplitudes were subject to decline. The two bar theories correctly predicted a decreasing likelihood of alternate bars throughout the experiment, mainly caused by the decline in channel slope that occurred in the first half of the experiment.

[48] The common practice in lowland stream restoration is the construction of a sinuous planform, with the aim of increasing the spatial flow variability, which is considered crucial for biodiversity within the stream. Alternate bars potentially have the same effect on the flow and are therefore sometimes considered to be an alternative, for the common practice within lowland stream restoration. We showed that the initial conditions, controlled by the channel slope, were favorable for the formation of alternate bars. A

Figure 16. Photos of alternate bar 2, taken at 520, 681, 821, and 938 days after the start of the experiment.

backwater curve, due to a narrow cross-sectional shape near the downstream end of the study reach, caused the channel slope to decline. After the channel slope declined, the conditions promoting bar development vanished. As a consequence, the regular pattern of alternate bars disappeared. The final channel slope of the presented case study is at the upper end of the range of slopes occurring in lowland streams. Therefore, stream restoration practitioners in lowland areas should not aim at autogenous development of alternate bars, but use other means for increasing the spatial flow variability. In other geographic regions, with steeper slopes and continuous sediment supply, alternate bars could be an alternative for the common practice of stream restoration.

[49] **Acknowledgments.** This study is part of a research project funded by the STOWA, the Foundation for Applied Water Research (Project code 443209), and by Water Board Aa en Maas. The contribution of the third author was supported by REFORM "Restoring Rivers for Effective Catchment Management" (EU FP7 grant 282656). We thank Mirja Kits, Chris van Rens, and Tom Basten (Waterboard Aa en Maas) for their continuing support to the project and for providing the aerial photos. We also thank Rob Fraaije (Utrecht University), Jan de Brouwer (Alterra), Matthijs Boersema, Johan Römelingh, and Philip Wenting (Wageningen University) for their contribution to the fieldwork campaign. And we thank Remko Uijlenhoet (Wageningen University), Piet Verdonschot (Alterra), the Associate Editor, and three anonymous reviewers for their comments on the manuscript.

References

Blondeaux, P., and G. Seminara (1985), A unified bar-bend theory of river meanders, *J. Fluid Mech.*, *157*, 449–470, doi:10.1017/S002211208500244.

Callander, R. A. (1969), Instability of river channels, *J. Fluid Mech.*, *36*(3), 465–480.

Church, M. A., and K. Road (1983), *Catalogue of alluvial river channel regime data,* Technical report, Dep. Geogr., Univ. British Columbia, Vancouver, B. C., Canada.

Colombini, M., and M. Tubino (1990), Finite amplitude multiple row bars: A fully non-linear spectral solution, in *Proceedings of Euromech 262*, edited by R. Soulsby and R. Bettess, pp. 163–169, Balkema, Rotterdam.

Colombini, M., G. Seminara, and M. Tubino (1987), Finite-amplitude alternate bars, *J. Fluid Mech.*, *181*, 213–232.

Crosato, A., and E. Mosselman (2009), Simple physics-based predictor for the number of river bars and the transition between meandering and braiding, *Water Resour. Res.*, *45*, W03424, doi:10.1029/2008WR007242.

Crosato, A., E. Mosselman, F. B. Desta, and W. S. J. Uijttewaal (2011), Experimental and numerical evidence for intrinsic nonmigrating bars in alluvial channels, *Water Resour. Res.*, *47*, W03511, doi:10.1029/2010WR009714.

Defina, A. (2003), Numerical experiments on bar growth, *Water Resour. Res.*, *39*(4), 1092, doi:10.1029/2002WR001455.

Deltares (2011), *SOBEK 2.12 User Manual*, Deltares, Delft, Netherlands.

Federici, B., and G. Seminara (2003), On the convective nature of bar instability, *J. Fluid Mech.*, *487*, 125–145, doi:10.1017/S0022112003004737.

Germanoski, D., and S. A. Schumm (1993), Changes in braided river morphology resulting from aggradation and degradation, *J. Geol.*, *101*(4), 451–466.

Hansen, E. (1967), On the formation of meanders as a stability problem, Prog. Rep. 13, Coastal Eng. Lab., Tech. Univ. of Denmark, Lyngby, Denmark.

Kleinhans, M. G., and J. H. van den Berg (2011), River channel and bar patterns explained and predicted by an empirical and a physics-based method, *Earth Surf. Processes Landforms*, *36*, 721–738, doi:10.1002/esp.2090.

Lanzoni, S. (2000), Experiments on bar formation in a straight flume, 1. Uniform sediment, *Water Resour. Res.*, *36*(11), 3337–3349.

Lewin, J. (1976), Initiation of bed forms and meanders in coarse-grained sediment, *GSA Bull.*, *87*(2), 281–285, doi:10.1130/0016-7606(1976)87¡281:IOBFAM¿2.0.CO;2.

Lisle, T. E., H. Ikeda, and G. Iseya (1991), Formation of stationary alternate bars in a steep channel with mixed-size sediment: A flume experiment, *Earth Surf. Processes Landforms*, *16*(5), 463–469, doi:10.1002/esp.3290160507.

Olesen, K. W. (1984), Alternate bars in and meandering of alluvial rivers, in *River Meandering, Proceedings of the Conference Rivers 1983*, edited by C. M. Elliott, pp. 873–884, American Society of Civil Engineers, New York.

Parker, G. (1976), On the cause and characteristic scales of meandering and braiding in rivers, *J. Fluid Mech.*, *76*(3), 457–480, doi:10.1017/S0022112076000748.

Parker, G., and H. Johannesson (1989), Observations on several recent theories of resonance and overdeepening in meandering channels, in *River Meandering, Water Resources Monograph*, vol. *12*, edited by S. Ikeda and G. Parker, pp. 379–415, AGU, Washington, D.C.

Poff, N. L., and J. V. Ward (1989), Implications of streamflow variability and predictability for lotic community structure: A regional analysis of streamflow patterns, *Can. J. Fish. Aquat. Sci.*, *46*(10), 1805–1818, doi:10.1139/f89–228.

Rodrigues, S., N. Claude, P. Jugé, and J. G. Bréheret (2012), An opportunity to connect the morphodynamics of alternate bars with their sedimentary products, *Earth Surf. Processes Landforms*, *37*, 240–248, doi:10.1002/esp.2255.

Schielen, R., A. Doelman, and H. E. de Swart (1993), On the nonlinear dynamics of free bars in straight channels, *J. Fluid Mech.*, *252*, 325–356.

Seminara, G., and M. Tubino (1989), Alternate bars and meandering: Free, forced and mixed interactions, in *River Meandering, Water Resources Monograph*, vol. *12*, edited by S. Ikeda and G. Parker, pp. 267–320, AGU, Washington, D.C.

Struiksma, N., K. W. Olesen, C. Flokstra, and H. J. De Vriend (1985), Bed deformation in curved alluvial channels, *J. Hydraul. Res.*, *23*(1), 57–79, doi:10.1080/00221688509499377.

Talmon, A. M., N. Struiksma, and M. C. L. M. van Mierlo (1995), Laboratory measurements of the direction of sediment transport on transverse alluvial-bed slopes, *J. Hydraul. Res.*, *33*(4), 495–517.

Tate, N., C. Brunsdon, M. Charlton, A. S. Fotheringham, and C. H. Jarvis (2005), Smoothing/filtering LiDAR digital surface models: Experiments with loess regression and discrete wavelets, *J. Geogr. Syst.*, *7*, 273–290, doi:10.1007/s10109-005-0007-4.

Tubino, M. (1991), Growth of alternate bars in unsteady flow, *Water Resour. Res.*, *27*(1), 37–52.

Tubino, M., R. Repetto, and G. Zolezzi (1999), Free bars in rivers, *J. Hydraul. Res.*, *37*(6), 759–775, doi:10.1080/00221689909498510.

Venditti, J. G., P. A. Nelson, J. T. Minear, J. Wooster, and W. E. Dietrich (2012), Alternate bar response to sediment supply termination, *J. Geophys. Res.*, *117*, F02039, doi:10.1029/2011JF002254.

Welford, M. R. (1994), A field test of Tubino's (1991) model of alternate bar formation, *Earth Surf. Processes Landforms*, *19*(4), 287–297, doi:10.1002/esp.3290190402.